Electronic Supplementary Information (ESI)

B_4C enhances the supported platinum DER/HER performance

*Yanfeng Li†, Shijie Zhang†, Weiwei Xu, Chenghang Jiang, Liangbin Shao, Shibin Wang, Jianguo Wang**

Institute of Industrial Catalysis, College of Chemical Engineering, State Key Laboratory Breeding Base of Green-Chemical Synthesis Technology, Zhejiang University of Technology, Hangzhou 310032 China.

†Y.F. Li and S.J. Zhang contribute to this work equally

*Correspondence and requests for materials should be addressed to J.G.W. (email: jgw@zjut.edu.cn).

1. Experimental section

1.1. Materials

Potassium hydroxide (KOH, 95%), Sodium hydroxide (NaOH, 95%), Boron carbide (B_4C, 99%) and Platinum (II) acetylacetonate ($Pt(acac)_2$, 97%) were obtained from Macklin Biochemical Co. Sulfuric acid (H_2SO_4, 95-98%) and Sodium (Na, 99.5%) was obtained from Sinopharm Group Chemical Reagent Co. Deuterium water (D_2O, 99.8%) was obtained from Shenzhen Ruilin Technology Co., Ltd. The commercial Pt/C (20 wt.%) was purchased from Alfa Aesar (China) Chemical Co., Ltd. Ethanol (Superdry, water < 50 ppm) was bought from Meryer Co., Ltd. Activated carbon (AR) was purchased from 9 Ding Chemistry Co., Ltd. Deionized water was prepared by HHitch laboratory water purification system. All chemicals were used as received without further purification.

1.2. Preparation of Pt/B_4C

7 wt. % Pt/B_4C catalyst was prepared by pyrolysis method. In general, 14.12 mg $Pt(acac)_2$ and 100 mg B_4C are mixed, then finely ground in an agate mortar, the powder is transferred to a crucible, which is finally placed in a tubular furnace in an argon atmosphere at a heating rate of 5°Cmin^{-1}. The powder obtained after annealing at 350°C for 3 h was named Pt/B_4C (or Pt/B_4C-350-3).

Similarly, the samples prepared by annealing at 150°C, 250°C, 450°C and 550°C for 3 h were named Pt/B_4C-150-3, Pt/B_4C-250-3, Pt/B_4C-450-3 and Pt/B_4C-550-3, respectively. In addition, the samples prepared by annealing at 350°C for 1h and 5h were named Pt/B_4C-350-1 and Pt/B_4C-350-5, respectively.

1.3. Preparation of Pt/AC

The 7 wt.% Pt/C catalyst was prepared by the pyrolysis method. Typically, 14.12 mg $Pt(acac)_2$ and 100 mg Carbon were mixed and fine ground by an agate mortar followed by the powder was transferred into a crucible. And then the pyrolysis was carried out at 350 °C (heating rate of 5 °C min^{-1}) for 3 h under Argon atmosphere. The final powder was collected and denoted as Pt/AC.

1.4. Preparation of the working electrode

4 mg Pt/B_4C was added into the mixture of 0.9 mL absolute ethanol and 0.1 mL of 5 wt.% Nafion solution. The catalyst solution was then sonicated for 30 min at room temperature. Afterward, 0.02 mL homogeneous solution was slowly dropped on a glassy carbon electrode (GCE, 4 mm in diameter) and dried under infrared light. The other electrodes were prepared by the same method. The working electrode used in the catalyst yield test was prepared by dropping 1 mL of ink solution onto a 1 × 1 cm carbon cloth under an infrared lamp.

1.5. Materials characterization

The morphology of samples was observed through a field emission scanning electron microscope (FE-SEM, HITACHI Regulus 8100) at an acceleration voltage of 20 kV. Transmission electron microscopy (TEM, Tecnai G2F30S-Twin) images were obtained at 300 kV by drop casting the sample dispersions on carbon-coated Cu grids and drying under ambient conditions. The powder X-ray diffraction (XRD, Bruker D8 Advance) was carried out with Cu-Kα radiation (40 kV and 40 mA, λ =0.1544 nm) in the 2θ range 5-90°. The X-ray photoelectron spectroscopy was measured by an X-ray photoelectron spectrometer (XPS, Thermo Scientific ESCALAB 250 Xi) with Al Kα radiation, the XPS data were normalized by using the binding energy value of adventitious carbon at 284.8 eV.

1.6. Electrochemical measurements and test condition

The electrochemical measurements were carried out by the CHI660D (CH Instruments, Inc., Shanghai) electrochemical workstation at room temperature. Specifically, the hydrogen evolution reaction (HER) and deuterium evolution reaction (DER) was tested using a standard three-electrode cell in 1 M NaOD/NaOH/KOH and 0.5M D_2SO_4/H_2SO_4 electrolyte solution with a GCE electrode as the working electrode (WE), a graphite rod electrode as the counter electrode (CE), Hg/HgO electrode as reference electrode (RE) in alkaline solution and Ag/AgCl electrode as reference electrode (RE) in acidic solution. The potential was converted to the reversible hydrogen electrode (RHE) using the following equation (Nernst equation):

E(RHE)= E(Hg/HgO) + 0.097 V + 0.059×pH.

E(RHE)= E(Ag/AgCl) + 0.197 V + 0.059×pH.

Cyclic voltammetry (CV) was performed in an alkaline solution over a potential range of 0.2 to -0.8 V (V vs.RHE) at a scan rate of 200 mV s^{-1}. Cyclic voltammetry (CV) was performed in an acidic solution over a potential range of 0.9 to -0.1 V (V vs.RHE) at a scan rate of 200 mV s^{-1}. Linear sweep voltammetry (LSV) measurements in alkaline solutions are performed over a potential range of -0.7 to -1.4 V at a scan rate of 5 mV s^{-1}. LSV measurements in acidic solutions are performed over a potential range of 0 to -0.7 V at a scan rate of 5 mV s^{-1}. Electrochemically active surface area (ECSA) was determined by electrochemical capacitance measurements at scan rates of 20 to 120 mV s^{-1}, and the potential range of ECSA in alkaline solution was -0.725 to 0.825 V. Potential of ECSA in acidic solution The test range is 0 to -0.1 V.

2. Computational methods

In this work, the periodic DFT calculations were implemented using the Vienna ab initio simulation package (VASP).[1, 2] The ion-electron interaction is described by applying the exchange-correlation function of the Perdew-Burke-Ernzerh of (PBE)[3] method and the projected augmented wave (PAW).[4, 5] The cut-off energy for the plane-wave basis sets was 400 eV. The electronic energy of the supercell was converged on 10^{-6} eV, with the force on each relaxed atom converged to 0.02 eV/Å in the ionic relaxation calculations, respectively. For the surface of Pt/B_4C, a 5×5×1 Monk horst-Pac-k k-mesh in the Brillouin zone was used for this structure relaxation.

Considering that Pt nanoparticles are greatly dispersed on the B_4C support, as displayed in Figure 1h. The single cell Pt with Fm3m space group is selected. To improve the stability and match of Pt, the (001) plane was taken and the cell was expanded to a 2×2 supercell. The lattice mismatch between Pt and B_4C is 2%, which can form a reasonable heterojunction. The Pt/B_4C was modeled by anchoring Pt metal atoms on the substrate in Figure. 3a. Among the B_4C of four surfaces (001) loaded with metal Pt. The vacuum space of 15 Å was added to the z-direction of the slab modules.

The thermodynamic stabilities of Pt/B_4C were estimated by the value of formation energy (E_f) as followings:

$$E_f = E_{Pt/B4C} - E_{B4C} - E_{Pt(001)}$$

where $E_{Pt/B4C}$ is the energy of the metal atoms embedded in B_4C. E_{B4C} and $E_{Pt(001)}$ are the energy of metal atoms in the bulk and the energy of B_4C supporter in the bulk.

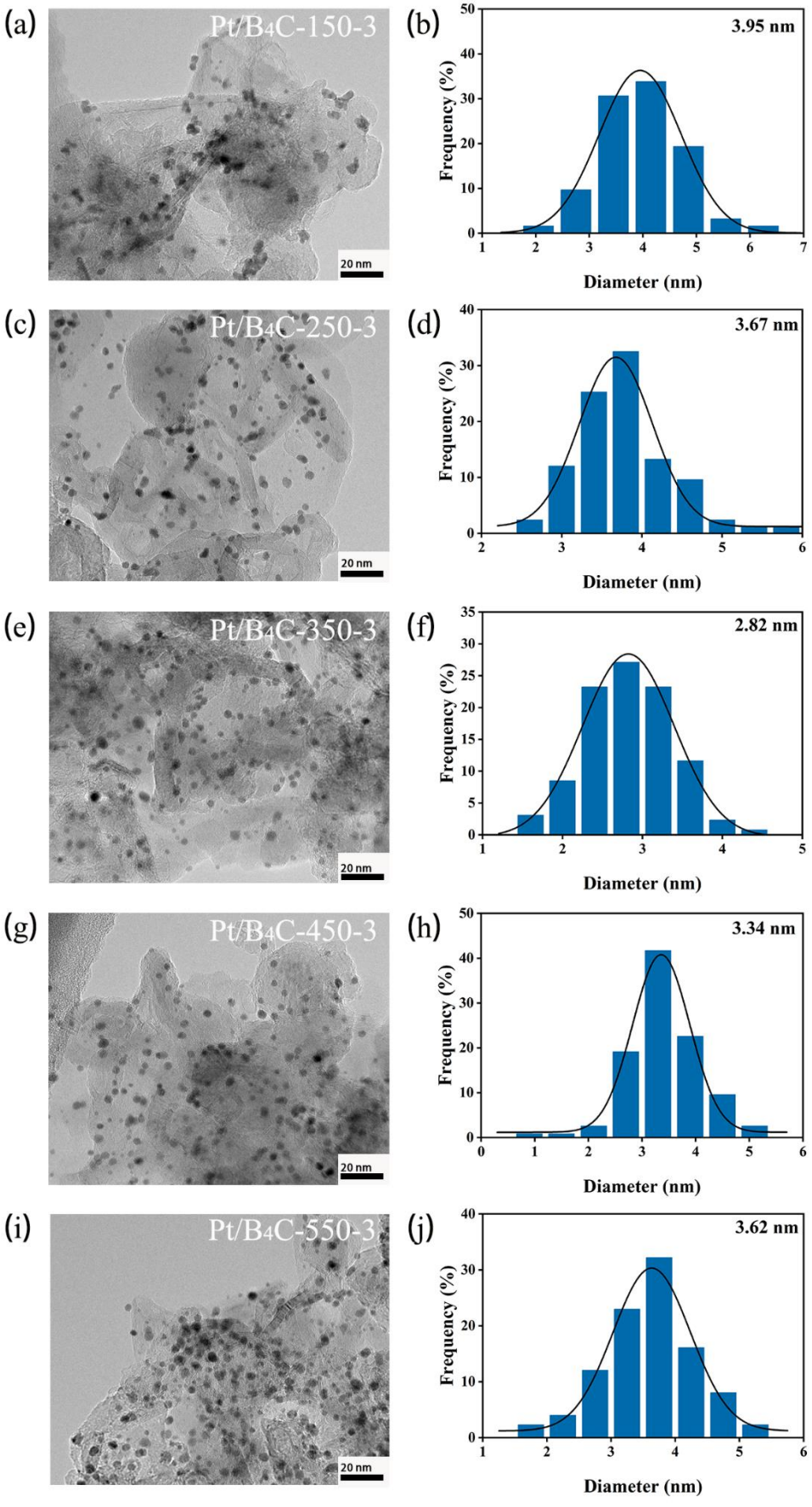
(a)
Pt/B4C-150-3
20 nm
(b)
3.95 nm
Frequency (%)
Diameter (nm)
(c)
Pt/B4C-250-3
20 nm
(d)
3.67 nm
Frequency (%)
Diameter (nm)
(e)
Pt/B4C-350-3
20 nm
(f)
2.82 nm
Frequency (%)
Diameter (nm)
(g)
Pt/B4C-450-3
20 nm
(h)
3.34 nm
Frequency (%)
Diameter (nm)
(i)
Pt/B4C-550-3
20 nm
(j)
3.62 nm
Frequency (%)
Diameter (nm)

Fig. S1. Pt/B_4C prepared at different annealing temperatures. (a) TEM image of Pt/B_4C-150-3, (b) Particle size statistics of Pt on Pt/B_4C-150-3 in Figure S1a. (c) TEM image of Pt/B_4C-250-3, (d) Particle size statistics of Pt on Pt/B_4C-250-3 in Figure S1c. (e) TEM image of Pt/B_4C-350-3, (f) Particle size statistics of Pt on Pt/B_4C-350-3 in Figure S1e. (g) TEM image of Pt/B_4C-450-3, (h) Particle size statistics of Pt on Pt/B_4C-450-3 in Figure S1g. (i) TEM image of Pt/B_4C-550-3, (j) Particle size statistics of Pt on Pt/B_4C-550-3 in Figure S1i.

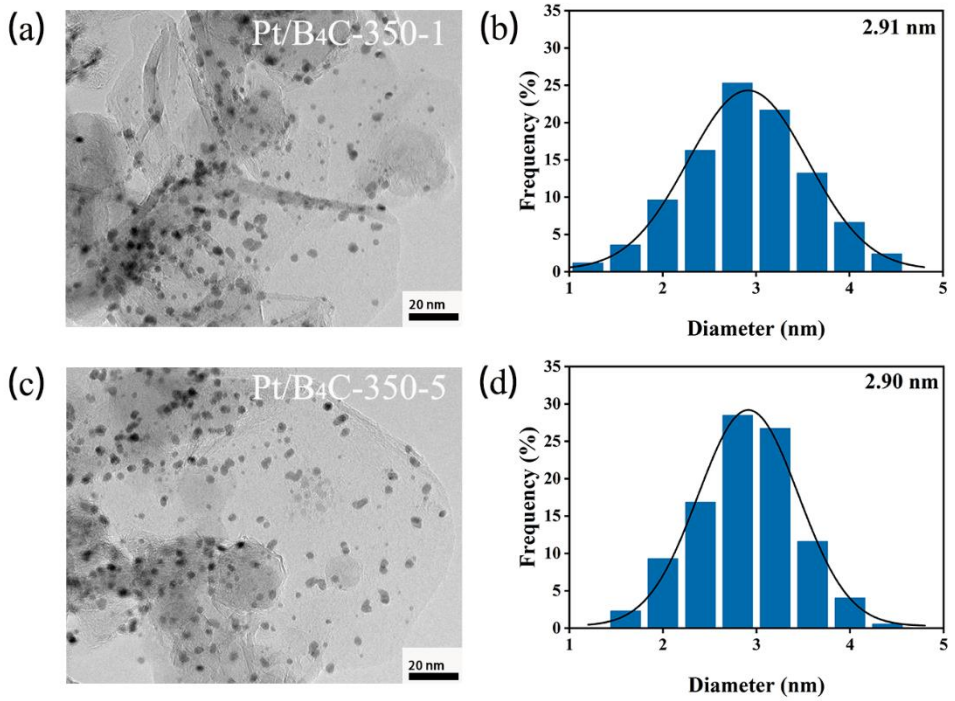

Fig. S2. Pt/B_4C prepared at different annealing times. (a) TEM image of Pt/B_4C-350-1, (b) Particle size statistics of Pt on Pt/B_4C-350-1 in Figure S2a. (c) TEM image of Pt/B_4C-350-5, (d) Particle size statistics of Pt on Pt/B_4C-350-5 in Figure S2c.

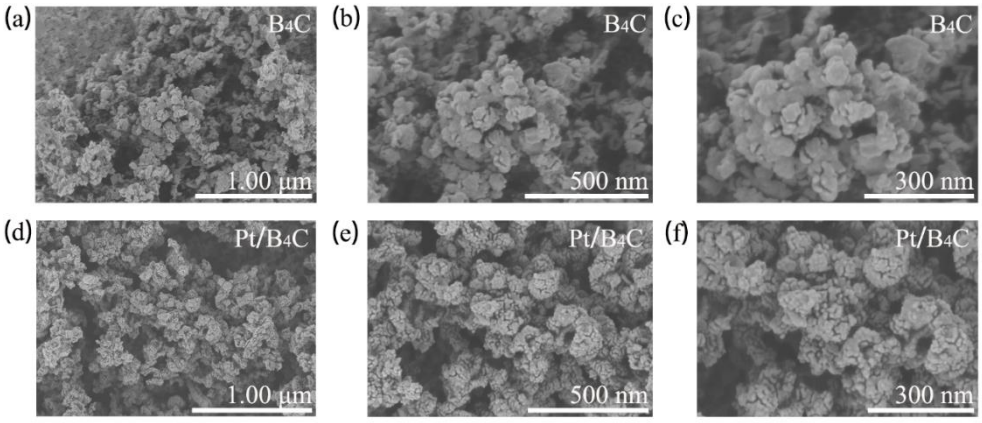

Fig. S3. (a-c) SEM image of B_4C, (d-f) SEM image of Pt/B_4C.

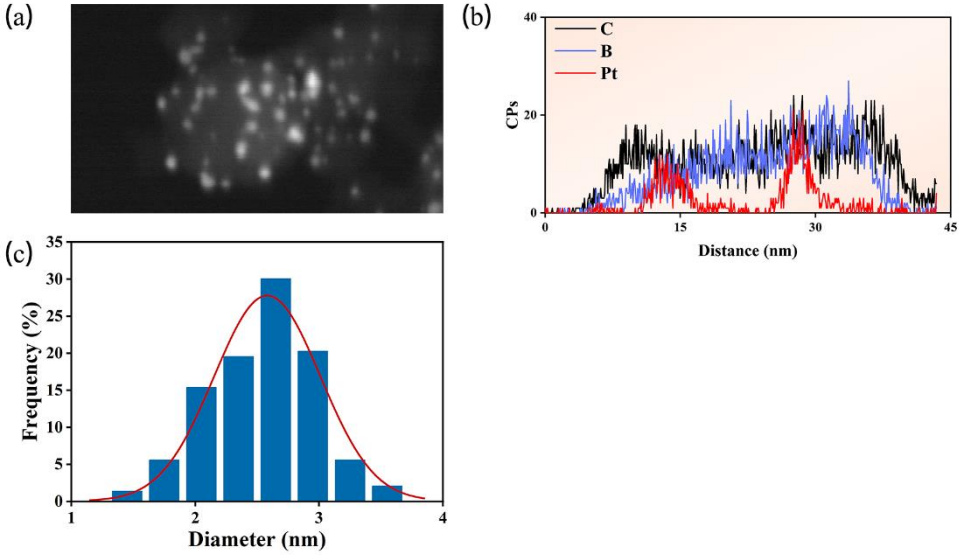

Fig. S4. (a) HAADF-STEM image of Pt/B_4C. (b) The cross-sectional compositional line profile. (c) Particle size statistics of Pt on Pt/B_4C in Figure 1g.

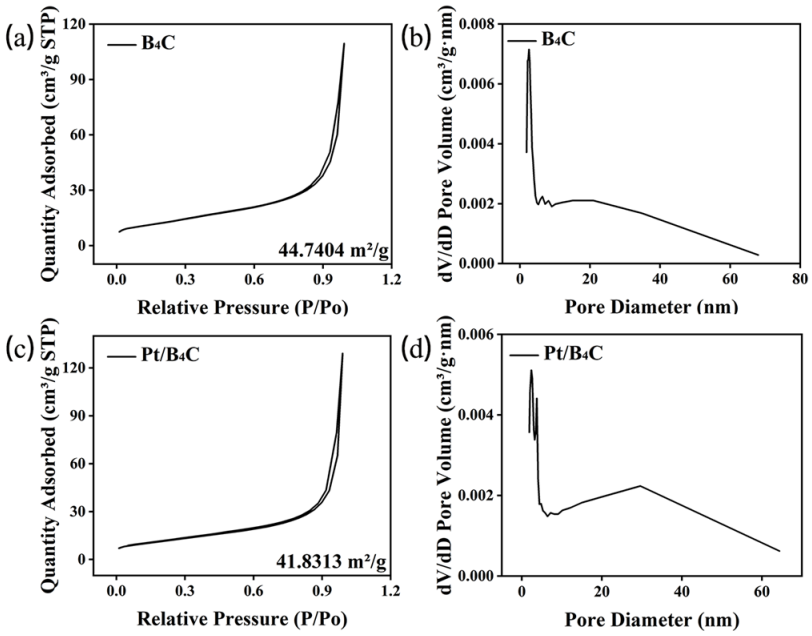

Fig. S5. The comparison graph of BET area and pore size change before and after catalyst preparation.

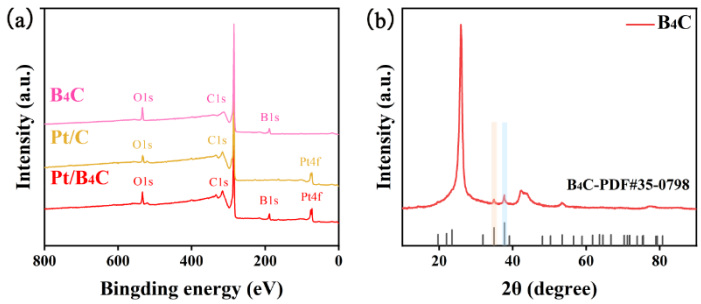

Fig. S6. (a) XPS Survey plots of Pt/B_4C, B_4C, and Pt/C, (b) XRD patterns for B_4C.

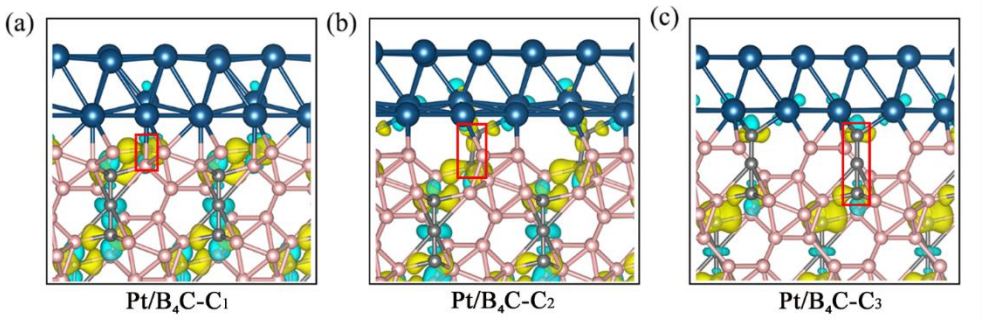

Fig. S7. Static deformation density map in the plane of different structural surfaces, with cyan and yellow representing the decrease and increase in electrons, respectively.

Table S1. Electron transfer in different Pt/B_4C structures

Heterojunction of different joint surfaces	Electron density transfer of carbon
Pt/B_4C-B	1.054931
Pt/B_4C-C_1	1.852046
Pt/B_4C-C_2	1.616787
Pt/B_4C-C_3	1.503081

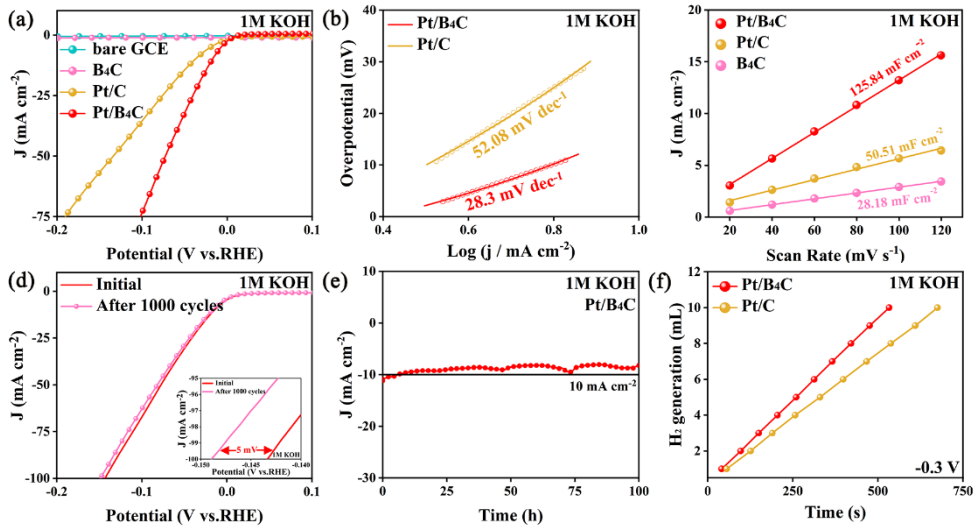

Fig. S8. Electrochemical performance of the Pt/B$_4$C in 1M KOH solution. (a) HER polarization curves of Pt/B$_4$C, B$_4$C, Pt/C, and bare GCE, respectively. (b) Tafel plots of Pt/B$_4$C and Pt/C, respectively. (c) ECSA of Pt/B$_4$C, B$_4$C, and Commercial Pt/C. (d) ADT test of Pt/B$_4$C at the range of 0.2 to -0.8 V in 1 M KOH. (e) Long-term durability test of Pt/B$_4$C. (f) Yield comparison test of Pt/B$_4$C and Pt/C.

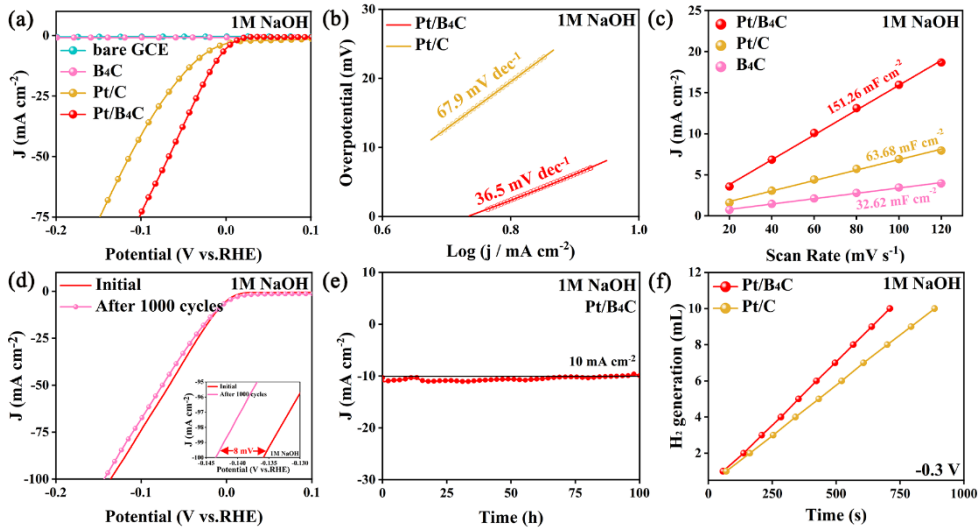

Fig. S9. Electrochemical performance of the Pt/B$_4$C in 1M NaOH solution. (a) HER polarization curves of Pt/B$_4$C, B$_4$C, Pt/C, and bare GCE, respectively. (b) Tafel plots of Pt/B$_4$C and Pt/C, respectively. (c) ECSA of Pt/B$_4$C, B$_4$C, and Commercial Pt/C. (d) ADT test of Pt/B$_4$C at the range of 0.2 to -0.8 V in 1 M NaOH. (e) Long-term durability test of Pt/B$_4$C. (f) Yield comparison test of Pt/B$_4$C and Pt/C.

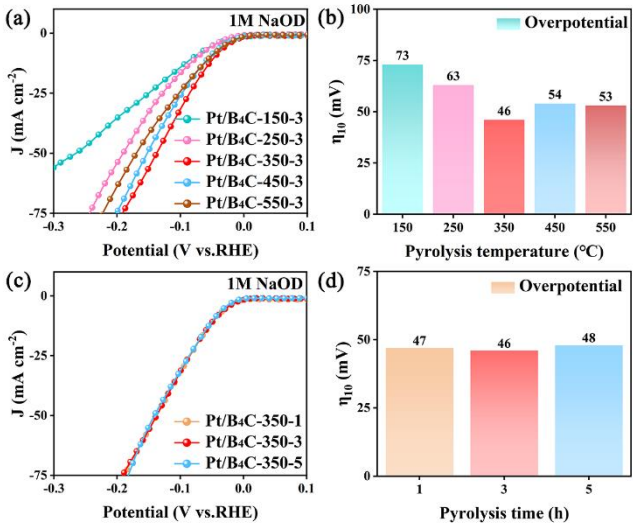

Fig. S10. Electrochemical polarization curves of Pt/B_4C catalysts prepared at different annealing temperatures and annealing times in 1 M NaOD solution.

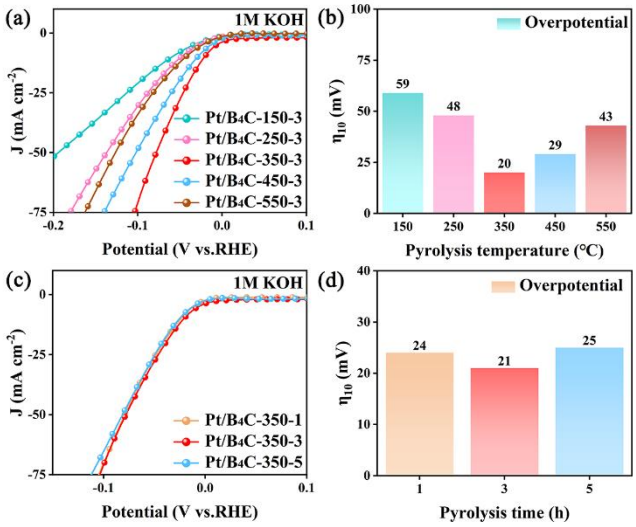

Fig. S11. Electrochemical polarization curves of Pt/B_4C catalysts prepared at different annealing temperatures and annealing times in 1 M KOH solution.

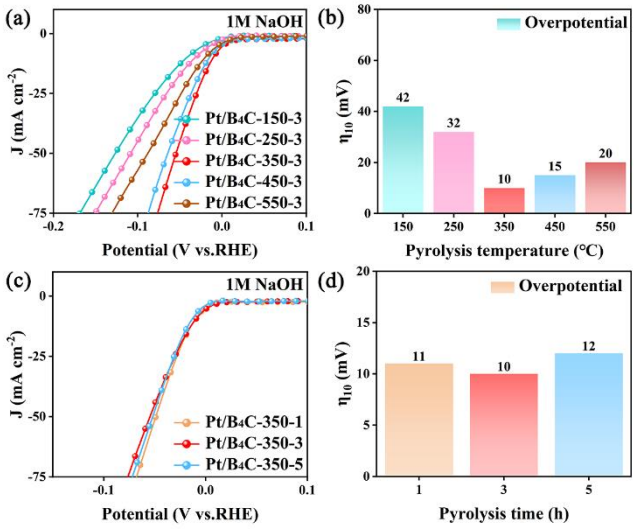

Fig. S12. Electrochemical polarization curves of Pt/B_4C catalysts prepared at different annealing temperatures and annealing times in 1 M NaOH solution.

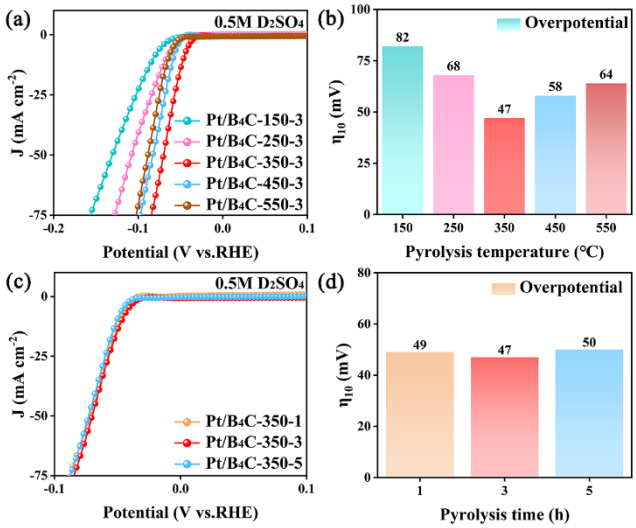

Fig. S13. Electrochemical polarization curves of Pt/B_4C catalysts prepared at different annealing temperatures and annealing times in 0.5 M D_2SO_4 solution.

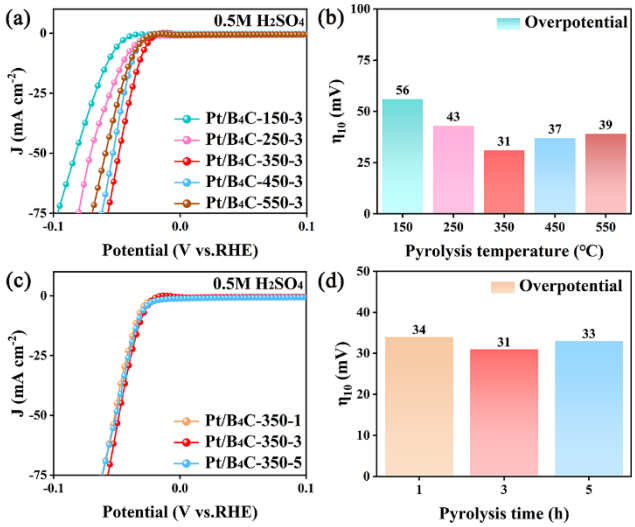

Fig. S14. Electrochemical polarization curves of Pt/B_4C catalysts prepared at different annealing temperatures and annealing times in 0.5 M H_2SO_4 solution.

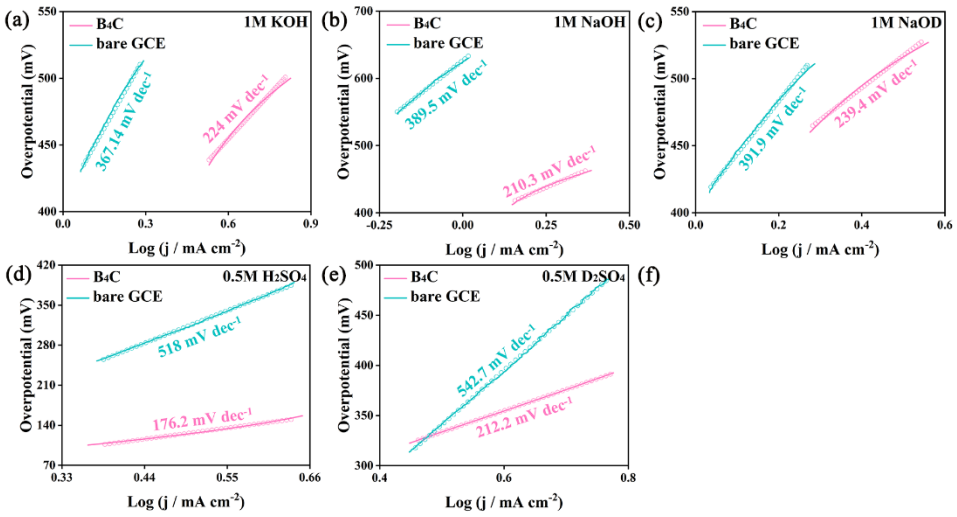

Fig. S15. Tafel plots of B_4C, and bare GCE.

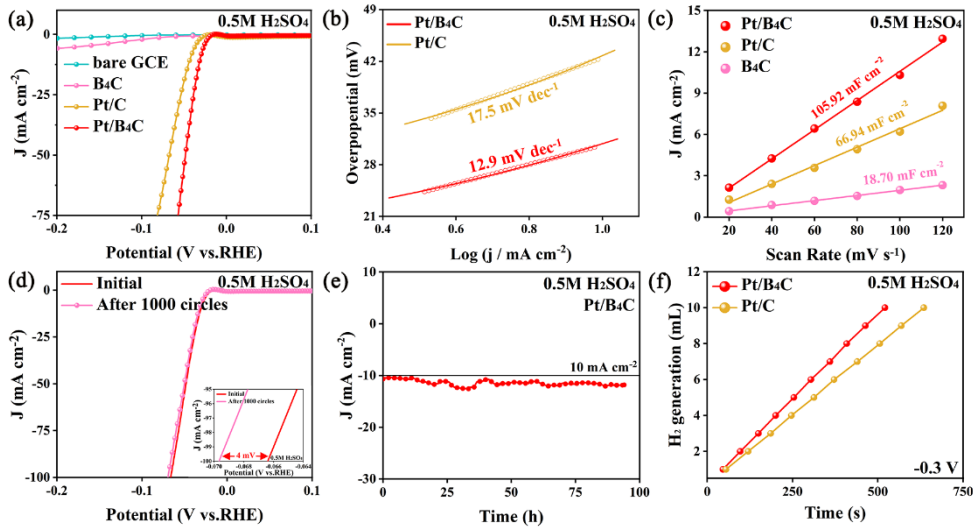

Fig. S16. Electrochemical performance of the Pt/B_4C in 0.5M H_2SO_4 solution. (a) HER polarization curves of Pt/B_4C, B_4C, Pt/C, and bare GCE, respectively. (b) Tafel plots of Pt/B_4C and Pt/C, respectively. (c) ECSA of Pt/B_4C, B_4C, and Commercial Pt/C. (d) ADT test of Pt/B_4C at the range of 0.9 to -0.1 V in 0.5 M D_2SO_4. (e) Long-term durability test of Pt/B_4C. (f) Yield comparison test of Pt/B_4C and Pt/C.

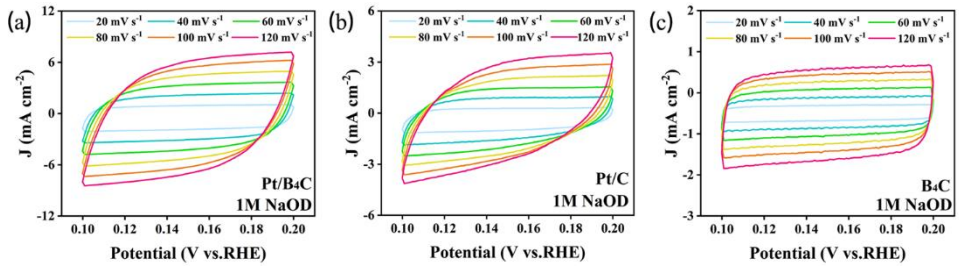

Fig. S17. The CV cycling curves of Pt/B_4C, Pt/C, and B_4C in 1 M NaOD solution at different scan rates ranging from 20 to 120 mV s^{-1}.

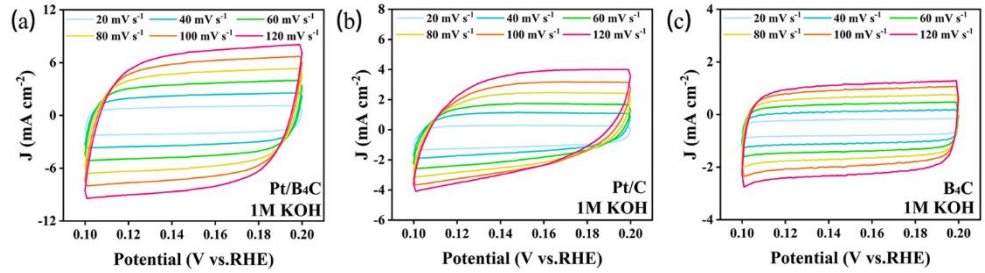

Fig. S18. The CV cycling curves of Pt/B_4C, Pt/C, and B_4C in 1 M KOH solution at different scan rates ranging from 20 to 120 mV s^{-1}.

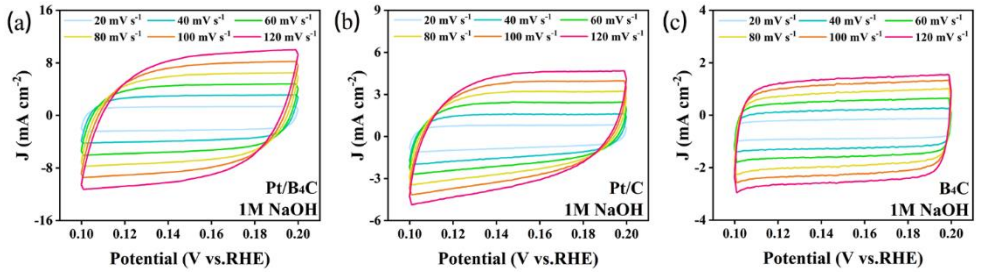

Fig. S19. The CV cycling curves of Pt/B_4C, Pt/C, and B_4C in 1 M NaOH solution at different scan rates ranging from 20 to 120 mV s^{-1}.

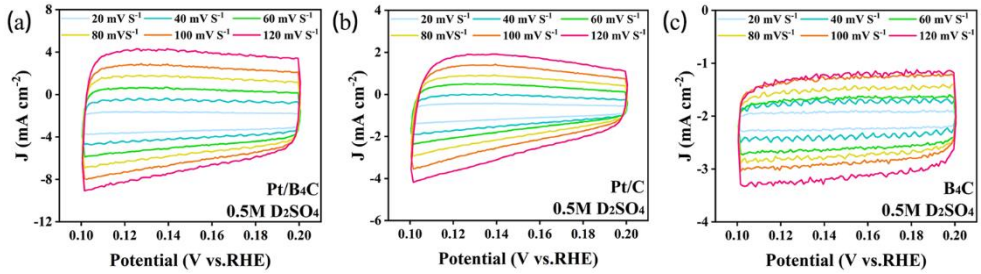

Fig. S20. The CV cycling curves of Pt/B_4C, Pt/C, and B_4C in 0.5 M D_2SO_4 solution at different scan rates ranging from 20 to 120 mV s^{-1}.

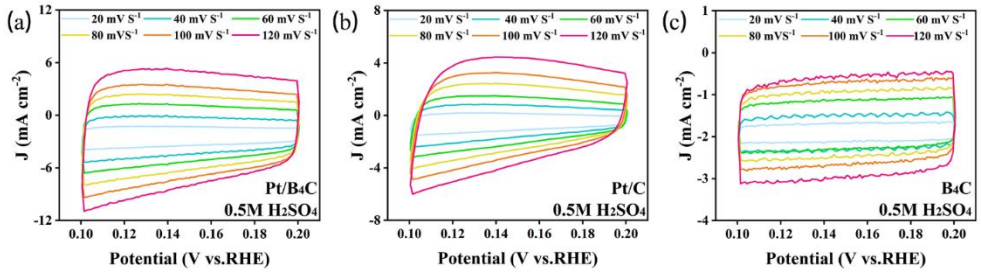

Fig. S21. The CV cycling curves of Pt/B_4C, Pt/C, and B_4C in 0.5 M H_2SO_4 solution at different scan rates ranging from 20 to 120 mV s^{-1}.

Table S2. Comparison of HER performance of Pt/B_4C with other reported Pt-based electrocatalysts in 1 M KOH.

Catalysts	Electrolyte	Overpotential at 10 mA cm^{-2} (mV)	Tafel slope (mV dec^{-1})	Ref.
Pt/B_4C	**1 M KOH**	**18**	**28.3**	**This work**
Pt/VG Ar-5	1M KOH	124	36	1[6]
(Ru-N)@Pt	1M KOH	15	25	2[7]
Pt-Co/CoO_x	1M KOH	28	29.3	3[8]
PtNi-NC-900	1M KOH	37.4	43.2	4[9]
d-Pt-Ni NWs	1M KOH	15	29	5[10]
10% NiOx@Pt/G	1M KOH	38.3	116	6[11]
Pt@Ni−Ni(OH)	1M KOH	27	50.7	7[12]
PtNiP-0.11 NWs	1M KOH	12	26.6	8[13]
Pt/NiFe-ED (300 μM)	1M KOH	17	45	9[14]
Pt_2Ni_3-PNWs	1M KOH	44	66	10[15]

Table S3. Comparison of HER performance of Pt/B_4C with other reported Pt-based electrocatalysts in 0.5 M H_2SO_4.

Catalysts	Electrolyte	Overpotential at 10 mA cm^{-2} (mV)	Tafel slope (mV dec^{-1})	Ref.
Pt/B_4C	**0.5 M H_2SO_4**	**31**	**12.9**	**This work**
Pt/R-NaxWO_3@SM-17	0.5 M H_2SO_4	20	18.6	11[16]
Pt-x -PVA	0.5 M H_2SO_4	34	31	12[17]
Pt-520/Au@MnO_2	0.5 M H_2SO_4	34	19	13[18]
Pt/NC-850	0.5 M H_2SO_4	17	32	14[19]
Pt-MoS_2	0.5 M H_2SO_4	67.4	76.2	15[20]
Pt/NP-CNTs	0.5 M H_2SO_4	25	28	16[21]
Pt/MIL-100(Fe)	0.5 M H_2SO_4	46	19.7	17[22]
$Pt_{61}La_{39}$@KB	0.5 M H_2SO_4	38	29	18[23]
Pt/Sv-MoS_{2-x}	0.5 M H_2SO_4	26.6	34.8	19[24]
Pt_1Ru_1/NMHCS-A	0.5 M H_2SO_4	22	38	20[25]

References

1. G. Kresse and J. Furthmüller, *Comput. Mater. Sci.*, 1996, **6**, 15-50.
2. G. Kresse and J. Furthmüller, *Phys. Rev. B.*, 1996, **54**, 11169-11186.
3. J. P. Perdew, K. Burke and M. Ernzerhof, *Phys. Rev. Lett.*, 1996, **77**, 3865-3868.
4. P. E. Blöchl, *Phys. Rev. B.*, 1994, **50**, 17953-17979.
5. G. Kresse and D. Joubert, *Phys. Rev. B.*, 1999, **59**, 1758-1775.
6. C. Tsounis, B. Subhash, P. V. Kumar, N. M. Bedford, Y. Zhao, J. Shenoy, Z. Ma, D. Zhang, C. Y. Toe, S. Cheong, R. D. Tilley, X. Lu, L. Dai, Z. Han and R. Amal, *Adv. Funct. Mater.*, 2022, **32**, 2203067.
7. M. Luo, J. Cai, J. Zou, Z. Jiang, G. Wang and X. Kang, *J. Mater. Chem. A.*, 2021, **9**, 14941-14947.
8. Y. Wang, W. Wu, R. Chen, C. Lin, S. Mu and N. Cheng, *Nano Res.*, 2022, **15**, 4958-4964.
9. J. Guo, J. Liu, X. Zhang, X. Guan, M. Zeng, J. Shen, J. Zou, Q. Chen, T. Wang and D. Qian, *J. Mater. Chem. A.*, 2022, **10**, 13727-13734.
10. Y. Xie, J. Cai, Y. Wu, X. Hao, Z. Bian, S. Niu, X. Yin, Z. Pei, D. Sun, Z. Zhu, Z. Lu, D. Niu and G. Wang, *ACS Mater. Lett.*, 2021, **3**, 1738-1745.
11. F. Kwofie, Y. Cheng, R. Zhang and H. Tang, *Materials Today Sustainability*, 2022, **19**, 100170.
12. D. Li, F. Liu, J. Dou and Q. Zhao, *ChemCatChem*, 2021, **13**, 5078-5083.
13. W. Lai, p. Yu, L. Gao, Z. Yang, B. He and H. Huang, *J. Mater. Chem. A.*, 2022, DOI: 10.1039/D2TA05156G.
14. Y. Feng, R. Ma, M. Wang, J. Wang, T. Sun, L. Hu, J. Zhu, Y. Tang and J. Wang, *J. Phys. Chem. Lett.*, 2021, **12**, 7221-7228.
15. P. Wang, Q. Shao, J. Guo, L. Bu and X. Huang, *Chem. Mater.*, 2020, **32**, 3144-3149.
16. J. Li, J. Wang, Y. Liu, C. Yuan, G. Liu, N. Wu and X. Liu, *Catal. Sci. Technol.*, 2022, **12**, 4498-4510.
17. Y. Qu, Z. Yu, D. Wei, L. Chen, Z. Zheng, N. Xiao, L. Wang and J. Yu, *Ionics*, 2021, **27**, 4885-4895.
18. T. Li, Y. Liu, R. Jia, M. Yaseen, L. Shi and L. Huang, *New J. Chem.*, 2021, **45**, 22327-22334.
19. G. Jiang, C. Zhang, X. Liu, J. Bai, M. Xu, Q. Xu, Y. Li, L. Long, G. Zhang, S. Li and Y. He, *Int. J. Hydrogen Energy*, 2022, **47**, 6631-6637.
20. A. Shan, X. Teng, Y. Zhang, P. Zhang, Y. Xu, C. Liu, H. Li, H. Ye and R. Wang, *Nano Energy*, 2022, **94**, 106913.
21. J. Han, C. Gong, C. He, P. He, J. Zhang and Z. Zhang, *J. Mater. Chem. A.*, 2022, DOI: 10.1039/D2TA05241E.
22. Z.-L. He, X. Huang, Q. Chen, C. Zhai, Y. Hu and M. Zhu, *J. Colloid Interface Sci.*, 2022, **616**, 279-286.
23. N. Nie, D. Zhang, Z. Wang, Y. Qin, X. Zhai, B. Yang, J. Lai and L. Wang, *Small*, 2021, **17**, 2102879.
24. F. Shi, W. Wu, J. Chen and Q. Xu, *Chem. Commun.*, 2021, **57**, 7011-7014.
25. W. Zhao, C. Luo, Y. Lin, G.-B. Wang, H. M. Chen, P. Kuang and J. Yu, *ACS Catal.*, 2022, **12**, 5540-5548.